



The effect of zirconium doping of cerium dioxide nanoparticles on pulmonary and cardiovascular toxicity and biodistribution in mice after inhalation

Susan Dekkers, Mark R. Miller, Roel P. F. Schins, Isabella Römer, Mike Russ, Rob J. Vandebriel, Iseult Lynch, Marie-France Belinga-Desaunay, Eugenia Valsami-Jones, Shea P. Connell, Ian P. Smith, Rodger Duffin, John A. F. Boere, Harm J. Heusinkveld, Catrin Albrecht, Wim H. de Jong & Flemming R. Cassee

To cite this article: Susan Dekkers, Mark R. Miller, Roel P. F. Schins, Isabella Römer, Mike Russ, Rob J. Vandebriel, Iseult Lynch, Marie-France Belinga-Desaunay, Eugenia Valsami-Jones, Shea P. Connell, Ian P. Smith, Rodger Duffin, John A. F. Boere, Harm J. Heusinkveld, Catrin Albrecht, Wim H. de Jong & Flemming R. Cassee (2017) The effect of zirconium doping of cerium dioxide nanoparticles on pulmonary and cardiovascular toxicity and biodistribution in mice after inhalation, *Nanotoxicology*, 11:6, 794-808, DOI: [10.1080/17435390.2017.1357214](https://doi.org/10.1080/17435390.2017.1357214)

To link to this article: <https://doi.org/10.1080/17435390.2017.1357214>



View supplementary material 



Accepted author version posted online: 25

Jul 2017.

Published online: 09 Aug 2017.



Submit your article to this journal 



Article views: 261



CrossMark

View Crossmark data 



Citing articles: 3 

ORIGINAL ARTICLE



The effect of zirconium doping of cerium dioxide nanoparticles on pulmonary and cardiovascular toxicity and biodistribution in mice after inhalation

Susan Dekkers^a, Mark R. Miller^b , Roel P. F. Schins^c , Isabella Römer^d , Mike Russ^e, Rob J. Vandebriel^a , Iseult Lynch^d , Marie-France Belinga-Desaunay^d, Eugenia Valsami-Jones^d , Shea P. Connell^b , Ian P. Smith^b, Rodger Duffin^b, John A. F. Boere^a, Harm J. Heusinkveld^{a,c} , Catrin Albrecht^c, Wim H. de Jong^a and Flemming R. Cassee^{a,f} 

^aNational Institute for Public Health and the Environment, Bilthoven, The Netherlands; ^bCentre for Cardiovascular Science & Centre for Inflammation Research, University of Edinburgh, Edinburgh, UK; ^cIUF – Leibniz Research Institute for Environmental Medicine, Düsseldorf, Germany; ^dSchool of Geography, Earth and Environmental Sciences, University of Birmingham, Birmingham, UK; ^ePromethean Particles Ltd., Nottingham, UK; ^fInstitute for Risk Assessment Sciences, Utrecht University, Utrecht, The Netherlands

ABSTRACT

Development and manufacture of nanomaterials is growing at an exponential rate, despite an incomplete understanding of how their physicochemical characteristics affect their potential toxicity. Redox activity has been suggested to be an important physicochemical property of nanomaterials to predict their biological activity. This study assessed the influence of redox activity by modification of cerium dioxide nanoparticles (CeO_2 NPs) via zirconium (Zr) doping on the biodistribution, pulmonary and cardiovascular effects in mice following inhalation. Healthy mice (C57BL/6J), mice prone to cardiovascular disease ($\text{ApoE}^{-/-}$, western-diet fed) and a mouse model of neurological disease ($5 \times \text{FAD}$) were exposed via nose-only inhalation to CeO_2 NPs with varying amounts of Zr-doping (0%, 27% or 78% Zr), or clean air, over a four-week period (4 mg/m³ for 3 h/day, 5 days/week). Effects were assessed four weeks post-exposure. In all three mouse models CeO_2 NP exposure had no major toxicological effects apart from some modest inflammatory histopathology in the lung, which was not related to the amount of Zr-doping. In $\text{ApoE}^{-/-}$ mice CeO_2 did not change the size of atherosclerotic plaques, but there was a trend towards increased inflammatory cell content in relation to the Zr content of the CeO_2 NPs. These findings show that subacute inhalation of CeO_2 NPs causes minimal pulmonary and cardiovascular effect four weeks post-exposure and that Zr-doping of CeO_2 NPs has limited effect on these responses. Further studies with nanomaterials with a higher inherent toxicity or a broader range of redox activities are needed to fully assess the influence of redox activity on the toxicity of nanomaterials.

ARTICLE HISTORY

Received 19 January 2017
Revised 7 June 2017
Accepted 3 July 2017

KEYWORDS

Nanomaterials; cerium dioxide; redox activity; inhalation; cardiovascular

Introduction

The amount and variety of nanomaterials developed, manufactured and used in different applications and commercial products is growing rapidly. Nanomaterials are of great interest because their physicochemical properties can be optimized to enhance their functionality in many different applications. However, the physicochemical properties that make nanomaterials so interesting may also lead to unexpected behavior and possible harmful effects in the environment and humans. To be able to better assess the potential risk of nanomaterials, more knowledge is needed on the possible toxicological consequences of their different (physicochemical) properties and their mechanisms of toxicity.

One of the key mechanisms of toxicity for nanomaterials is believed to be their ability to generate reactive oxygen species (ROS) (Miller et al., 2012; Unfried et al., 2007). After saturation of compensatory mechanisms, excessive cellular ROS can lead to oxidative stress, resulting in detrimental effects on cell function. In addition, amplification of inflammatory responses may occur that can exacerbate a number of diseases, such as cancer, cardiovascular diseases, neurodegenerative diseases and diabetes (Pisoschi & Pop, 2015). Nano-sized metal oxides are known to facilitate the formation

of ROS by depleting electrons from cellular redox species (cellular components able to release electrons) or by serving as catalysts in ROS production through the Fenton reactions, Fenton-like reactions, or the Haber–Weiss cycle reaction (Fu et al., 2014).

While there are clear associations between ROS generation and the toxicity of nanomaterials, comparisons between nanomaterials are complicated by the use of different core chemistries that will manifest as differences in other physicochemical properties in addition to redox activity. In the current study we applied chemical doping (intentional substitution of one element by another while maintaining the lattice structure and arrangement) of a single type of nanoparticle to specifically investigate the influence of redox activity on ROS formation, and associated induction of oxidative stress responses in mice *in vivo* after inhalation exposure. CeO_2 was selected as a nanomaterial that could be chemically modified appropriately and for which acute and subacute toxicity data from inhalation exposure was available (Aalapati et al., 2014; Demokritou et al., 2013; Gosens et al., 2014; Keller et al., 2014; Morimoto et al., 2015; Srinivas et al., 2011).

CeO_2 NPs are used in variety of applications, such as electrochemical sensors, fuel cells, reforming catalysts, as well as a diesel

CONTACT Susan Dekkers  susan.dekkers@rivm.nl  Centre for Sustainability, Environment and Health (DMG), National Institute for Public Health and the Environment (RIVM), P.O. Box 1, 3720 BA, Bilthoven, The Netherlands

 Supplemental data for this article can be accessed [here](#).

© 2017 Informa UK Limited, trading as Taylor & Francis Group

fuel additive used to increase engine efficiency and reduce particulate exhaust emissions (Cassee et al., 2011, 2012, Dunnick et al., 2016). Previous *in vitro* studies using pure CeO₂ NPs have shown contradicting results in terms of the oxidative stress impacts of CeO₂ NPs (Dunnick et al., 2015; Leung et al., 2015; Pesic et al., 2015). Some studies have found CeO₂ NPs to induce ROS and oxidative stress (Eom & Choi, 2009; Lin et al., 2006; Park et al., 2008), while others show protective effects against oxidant-induced apoptosis (Celardo et al., 2011; Xia et al., 2008). Differences in the CeO₂ NPs valence state in terms of the 3⁺:4⁺ ratio, or the proportion of the valence state at the NP surface, could account for some of these inconsistencies. Ce has the ability to shift between a 3⁺ and 4⁺ valence state. The antioxidant properties of CeO₂ NPs are due to its ability to scavenge free radicals, which is accomplished through its ability to switch from the 3⁺ to the 4⁺ valence state (Hirst et al., 2009). The antioxidant efficacy of CeO₂ NPs can be enhanced by incorporation of Zr in the CeO₂ lattice (Tsai et al., 2008).

In this study, different quantities of Zr were incorporated into the crystalline structure of the CeO₂ NPs in an attempt to generate CeO₂ NPs with different antioxidant potentials. The Zr-doped CeO₂ NPs were produced through an industrial collaboration and therefore had a real-life application. Furthermore, the CeO₂ structure could tolerate Zr substitution at a range of concentrations, allowing for a precise control of the particle redox state. The aim of our study was to investigate if the modification of the redox activity of CeO₂ NPs by Zr-doping influences their pulmonary and cardiovascular effects in mice following subacute inhalation exposure. We hypothesized that the adverse biological effects of CeO₂ NPs can be diminished by Zr-doping, due to an increased antioxidant potential of the doped nanoparticles.

The study was conducted in three different mouse models to explore the (patho)physiological effects of nanoparticle exposure on multiple organ systems. This paper describes the biodistribution, pulmonary and cardiovascular findings whereas the neurological data will be published in a separate paper.

Materials and methods

Study design

To explore the (patho)physiological effects of nanoparticle on multiple organ systems, three different mouse models were exposed.

Atherosclerosis-prone apolipoprotein E-deficient (ApoE^{−/−}) mice are a well-established model for the study of the vascular disease atherosclerosis (Coleman et al., 2006), a disease characterized by the build-up of lipid- and inflammatory cell-rich plaques within arteries, which underlies the majority of cardiovascular diseases. The four-week exposure protocol was integrated into an eight-week high-fat feeding regime that has been shown to generate complex atherosclerotic plaques with many of the hallmarks of the human disease in specific arterial locations (Cassee et al., 2012; Miller et al., 2013). ApoE^{−/−} mice were used to study hematology, pulmonary and cardiovascular effects.

The 5 × FAD mice are an Alzheimer's disease mouse model. Although these mice were included to study neurological effects that will be published in a separate paper, the hematology and pulmonary effects were also studied within the same animals and reported in this paper.

C57BL/6J mice were used as the background (non-genetically modified) strain of the disease mouse models and used to study biodistribution, hematology and pulmonary effects.

Hematology, pulmonary and cardiovascular effects were assessed four weeks post-exposure. This period was included,

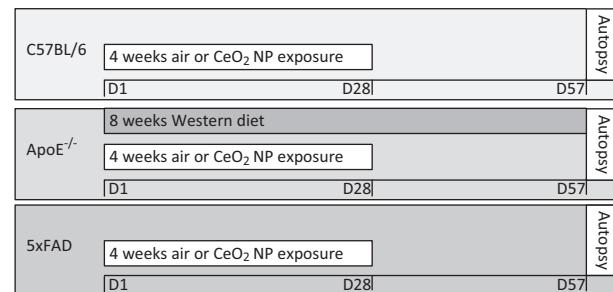


Figure 1. Schematic overview of the study design. D = day. D1–D28 = exposure period and D29–D57 = recovery period.

firstly, to provide the extra four weeks necessary for mice to develop sufficient plaque formation in arteries and secondly, to investigate the persistency of the pulmonary and cardiovascular effects.

Three groups of each mouse model were exposed to CeO₂ NPs with different amounts of Zr-doping and one control group to clean air. The number of animals per group was different for each of the mouse models, to provide sufficient statistical power to detect differences between exposed and control animals in the most important effect parameter of each mouse model. Based on previous experiments, 8 ApoE^{−/−} mice per group were expected to be sufficient to detect statistically significant differences in atherosclerotic plaque size and 5 C57BL/6J mice per group were expected to be sufficient to detect statistically significant differences in the number of neutrophils in the bronchoalveolar lavage fluid (BALF). However, 10 C57BL/6J mice per group were included, since 10 C57BL/6J mice per group and 16 5 × FAD mice per group were needed to provide sufficient statistical power in the neurological study. Mice were exposed nose-only for four weeks to 4 mg/m³ NP for 5 days/week for 3 h/day. This dose was primarily based on another four-week inhalation study in which inflammatory responses in the lungs of CD-1 mice were observed after exposed to 2 mg/m³ CeO₂ NPs for 5 days/week for 6 h/day (Aalapati et al., 2014). Effects were assessed 4 weeks post the final exposure (56 days after the initial exposure). A schematic overview of the experimental design is presented in Figure 1.

Nanomaterial production and characterization

To modify the redox activity, CeO₂ NPs were doped with different amounts of Zr (as per Table 1, Zr contents in the doped NPs were 27 mol% and 78 mol%). Addition of Zr into the crystalline structure of CeO₂ NPs is expected to enhance the antioxidant efficacy of CeO₂ NPs (Tsai et al., 2008).

CeO₂ NPs and Zr-doped CeO₂ NPs were produced using supercritical water hydrothermal synthesis (Cabanias et al., 2000). Briefly, H₂O was pumped through a pre-heating coil, heated to approximately 400 °C, brought into contact with a concurrently flowing solution of metal salts at room temperature (RT), while maintaining the flow rates, temperature and pressure constant. The mixture was cooled immediately after the mixing point and passed through a 7-μm filter to remove large aggregates. The solids in the aqueous suspensions were recovered by allowing the suspension to settle and drying at approximately 100 °C. The NPs were tested for endotoxin contamination using a limulus amoebocyte lysate (LAL) test. No endotoxin was detected in any of the NP suspensions.

To determine the Ce³⁺/Ce⁴⁺ ratio of the different NPs, ultraviolet-visible spectrophotometry (UV-vis) analysis was performed on 200 mg/L particle solutions, diluted in MilliQ water, with a 6800

Table 1. Physicochemical characteristics of the nanoparticles.

Characteristic	Method	Nanoparticle		
		CeO ₂	27% Zr-doped CeO ₂	78% Zr-doped CeO ₂
Primary particle size (mean \pm SD) (nm)	STEM-EELS	4.7 \pm 1.4	4.6 \pm 1.4	4.7 \pm 1.4
Ce ³⁺ /Ce ⁴⁺ ratio	UV-vis	0.87	0.98	1.4
Scavenging capacity ROS (Mean \pm SD) (% reduction compared to signal without NPs)	ESR	46 \pm 26	44 \pm 21	56 \pm 23
Median particle diameter at 128 μ g/ml in water (mean \pm SD)(nm)	DCS	39	40	41
Median particle diameter at 20 μ g/ml in water (mean \pm SD)(nm)	DLS	54 \pm 9	45 \pm 5	52 \pm 6
Median particle diameter at 1 mg/ml in water (mean \pm SD)(nm)	DLS	172 \pm 2	297 \pm 4	358 \pm 6
zeta potential at 1 mg/ml in water (mV \pm SD)		PDI: 0.27 \pm 0.01	PDI: 0.47 \pm 0.01	PDI: 0.49 \pm 0.03
EC ₂₀ cytotoxicity in A549 (Mean \pm 90% CI) (μ g/cm ²)	WST-1	50.3 \pm 0.7	45.9 \pm 3	44.1 \pm 2
		0.2 (0.0-23)	9 (0.0-38)	33 (0.1-68)

STEM-EELS: scanning transmission electron microscope (STEM)-electron energy loss spectroscopy (EELS) analysis; UV-vis: ultraviolet-visible spectrophotometry; ESR: electron-spin resonance; DCS: differential centrifugal sedimentation; DLS: dynamic light scattering; WST-1: water-soluble tetrazolium-1; EC₂₀: effective concentration resulting in 20% cytotoxicity.

Jenway double beam UV-vis spectrophotometer, with long path UV-vis cell cuvettes. The UV-vis absorption spectra were collected over a wavelength range of 200–700 nm. Both valence states of Ce strongly absorb ultraviolet light and each one has a characteristic spectrophotometric absorbance peak, with Ce³⁺ absorbing in the 230–260 nm range and Ce⁴⁺ absorbing in the 300–400 nm range.

Zr-doping of CeO₂ NPs might also cause differences in other characteristics than redox activity which can also influence the toxicity of the NPs, such as particle size distribution, aggregation, agglomeration and corona formation. Therefore the hydrodynamic size distributions and zeta potential were assessed using differential centrifugal sedimentation (DCS) and dynamic light scattering (DLS) analyzes. In addition, the effect of Zr-doping on the scavenging capacity of the CeO₂ NPs was investigated with electron-spin resonance (ESR). Before testing the NPs *in vivo*, the effect Zr-doping of CeO₂ NPs on the *in vitro* cytotoxicity was investigated in lung epithelial cells.

The scavenging capacity of ROS was investigated with ESR analysis using a cell free system with a 5,5-dimethyl-1-pyrroline N-oxide (DMPO) spin trap (He et al., 2014) in combination with hydrogen peroxide (H₂O₂) and copper sulfate (CuSO₄). The nanoparticle suspensions were thoroughly vortexed and sonicated for 5 min at RT in a sonication bath to re-disperse any agglomerates. A sample was made of 12.5 μ L nanoparticle suspension (1.28 mg/mL), 12.5 μ L CuSO₄ (20 μ M), 25 μ L H₂O₂ (0.5 M) and 50 μ L DMPO (0.05 M). This sample was incubated in a shaker water bath at 37 °C for 15 minutes at 100 rpm, vortexed and taken up in a capillary tube which was then sealed at the bottom with hematocrit and measured with the ESR Spectroscope (Miniscope MS 400; MT MagnetTech GmbH).

The effect of Zr-doping on *in vitro* cytotoxicity was tested in human lung epithelial carcinoma cells (A549) cells obtained from ATCC (VA, USA). A549 cells were cultured in tissue culture flasks in RPMI 1640 medium with Glutamax (Gibco; ThermoFisher Scientific Inc., Landsmeer, the Netherlands) supplemented with 10% Fetal Bovine Serum (FBS; Greiner BioOne BV, Alphen aan de Rijn, the Netherlands) and 1% penicillin/streptomycin (Gibco). Cells were cultured at 37 °C in a humidified atmosphere of 5% CO₂ in air. Twenty-four hours before exposure, the cells were harvested by a short incubation with 0.5% ethylenediaminetetraacetic acid (EDTA) trypsin in Ca/Mg free Dulbecco's Phosphate Buffered Saline (Gibco) and counted. Fifty thousand (5 \times 10⁴) cells were seeded in 96-well plates in 200 μ L cell culture medium per well. After 24 h of incubation a semi confluent monolayer of cells was obtained and the cells were exposed to 0, 1.25, 2.5, 5, 10, 20, 40 or 80 μ g/cm² of the various NPs in cell culture medium. Additional wells with the same concentrations of NPs in cell culture medium, but no A549 cells were included to measure possible interference of the

materials with the viability assay. Cell viability (i.e. cytotoxicity) was determined after 24 h of exposure by a colorimetric assay using cell proliferation reagent WST-1 (water-soluble tetrazolium-1) (Roche; Sigma-Aldrich Chemie). Dose-response modeling and derivations of the EC₂₀ (effective concentration resulting in 20% cytotoxicity) were performed using PROAST software (Slob, 2002) version 63.5.

Animals

Specific pathogen free (SPF) female ApoE^{−/−} mice ($N=32$; Taconic, Denmark) were obtained at age 10–12 weeks at the beginning of the study. The 5 \times FAD and C57BL/6J mice originated from Jackson Laboratories. For this study, female 5 \times FAD mice ($N=64$) and female wild type (WT) cross bread C57BL/6J littermates ($N=40$) were used at the age of 8–11 weeks. The mice were barrier maintained and housed in a single room in macrolon cages. The temperature and the relative humidity were controlled at 22 \pm 2 °C and at 40–70%, respectively. Lighting was artificial with a sequence of 12 h light and 12 h dark (at night). Feed and drinking water was provided *ad libitum* from the arrival of the mice until the end of the study, except during exposure. The ApoE^{−/−} mice were fed a commercially available rodent Western (high fat) diet (Purified Diet Western 4021.06; ABdiets, Woerden, The Netherlands), starting at the first day of the exposure period until the end of the experiment. The other mice were fed a standard commercially available rodent diet (SMR-A; ABdiets, Woerden, The Netherlands). Animals were monitored by cage-side observations and, if necessary, handled to detect signs of compromised health. The body weight of each animal was recorded one day before the start of exposure (day -1), prior to exposure on the first day and weekly thereafter. Experiments were conducted at Intravacc (Bilthoven, The Netherlands) under a protocol approved by the Ethics Committee for Animal Experiments of the RIVM and performed according to applicable national and EU regulations.

Inhalation exposure

Approximately one week before the four-week exposure period, 20 samples of each nanoparticle (one for each day) with a concentration of 1 mg/mL were prepared from the stock dispersions (20, 20 or 29 mg/mL for 0%, 27% and 78% Zr-doped CeO₂ NPs, respectively) by diluting with ultrapure water to the desired concentration. Stock and sample dispersions were sonicated for 5 min in an ultrasonic bath (Branson CPX2800, 40 kHz, 110 W) before use to re-disperse any possible agglomerates. Freshly generated aerosols of NPs were generated using a spray nozzle technique, diluted with pressurized clean particle-free air, and heated to

24–25 °C. Exposure was controlled based on stable particle number counts, mass concentrations, temperature and relative humidity, measured continuously using a condensation particle counter (CPC 3022 A from TSI Inc., St. Paul, MN, USA), a tempered element oscillating microbalance (TEOM series1400A from Rupprecht & Patashnick, NY, USA) and M-170 Measurement Indicator (Vaisala M170; Vaisala Oyj, Helsinki, Sweden), respectively, during each exposure period. In addition, the test atmosphere is characterized at least twice during each exposure session using an optical particle sizer (OPS 3330; TSI Inc., St. Paul, MN, USA) and a scanning mobility particle sizer (SMPS 3936 from TSI Inc., St. Paul, MN, USA). The total mass concentration generated over the 3-h exposure period was determined by gravimetric analysis of pre-weighed and post-weighed polytetrafluoroethylene (PTFE) filters (Teflo R2PJO47, Pall corporation, Port Washington, NY, USA) using a micro-balance (Mettler MC or ME-5 microbalance; Mettler-Toledo LLC, Columbus, OH, USA). The count median diameter (CMD) and the mass median diameter (MMD) were estimated using the Aerosol Instrument Manager Software (Release Version 9.0.0.0, 15:32:53; Nov 11 2010 from TSI Inc., St Pauls, MN, USA), assuming spherical aggregation around primary particles of 4.7 ± 1.4 nm. In addition, aerosols were collected on polycarbonate filters for scanning electron microscopy (SEM) analysis. The SEM samples were prepared by placing a small piece of the filter on the SEM stub and coating it with platinum, and visualizing with an XL30 Environmental SEM-FEG microscope (Philips XL30 ESEM-FEG). During the 3 h exposure periods to the different nanoparticles, the control groups were exposed to filtered air under the same conditions (nose-only tubes) for the same amount of time.

Estimated deposited dose in lungs

To estimate the deposited dose in the lungs, the multiple path particle dosimetry model (MPPD v3.04[©] 2016 by Applied Research Associates, Inc., Albuquerque, NM, USA) was used. Default parameters for the B6C3F1 mouse were applied (forced respiratory capacity: 0.3 mL, upper respiratory tract volume: 0.0322 mL, nasal breathing, breathing frequency: 353/min, tidal volume: 0.20 mL, inspiration fraction: 0.5, no pause fraction). Calculations were performed using the count median diameter, geometric standard deviation and mass concentration of the exposure characterization and a density of 7.215 g/cm³ for CeO₂, 6.801 g/cm³ for 27% Zr-doped CeO₂ and 6.018 g/cm³ for 78% Zr-doped CeO₂ NPs.

Quantification of Ce and Zr in tissues

During necropsy, organs from half of the C57BL/6J mice per group were obtained to evaluate the distribution of the NPs throughout the body. Liver, spleen, kidneys, heart and right (exposed mice) or left (control mice) lung, were weighed and immediately frozen in liquid nitrogen for determination of the Ce and Zr concentrations. To allow measurement of multiple parameters within the same animal, different parts of the lungs were selected for the exposed compared to the control animals. From the exposed groups the right lung was used for quantification of Ce and Zr, because the left lung was needed for histopathological examination. From the control group the left lung was used for quantification of Ce and Zr, because the right lung was needed for bronchoalveolar lavage. The organs were digested by acidification of each sample with 2 mL nitric acid for 12 h. Hydrogen fluoride (0.2 mL) was added, followed by microwave heating for 45 min up to 185 °C, and maintained for a further 20 min. Boric acid (2 mL) was added to neutralize the hydrogen fluoride, and the samples were re-heated for 20 min to 160 °C, and maintained for 10 min. Once cooled, samples were filtered with a 450 nm syringe

filter, diluted with 10 mL deionized water and stored at room temperature (RT). The presence of Ce and Zr in the lungs, liver, spleen, kidneys and heart was determined by inductively coupled plasma mass spectrometry (ICP-MS) using a Perkin Elmer NexION 300× instrument operated in standard mode for Ce and Zr. The isotopes measured were ⁹⁰Zr and ¹⁴⁰Ce using ¹¹⁵In and ¹⁵⁹Tb as internal standards. Calibration standards (0–100 µg/L) were prepared from VWR 1000 mg/L stock solutions. Quantities are expressed as µg/g organ tissue.

Necropsy

Hematology

Animals were anesthetized with a mixture of ketamine and xylazine. Two blood samples were taken by eye extraction. The first sample was collected in a K3-EDTA tube (Minicollect K3EDTA, 1 mL, 450474 Greiner Bio-One) for hematological parameters as determined in a blood auto analyzer (ADVIA 2120 Hematology System; Siemens Healthineers, Erlangen, Germany) within 3 h after collection. The second sample was collected in a serum tube, which was kept for at least 30 min at RT before centrifugation at 2000g for 10 min at 20 °C. Serum was divided into separate aliquots of 50 µL and stored at –20 °C for further analysis.

Bronchoalveolar lavage

Lung lavage was performed at necropsy. A cannula was placed in the trachea and the diaphragm opened to decrease the amount of air inside the lungs. For the control animals and all ApoE^{–/–} animals, the right lung half was rinsed twice with approximately 0.5 mL (26.7 mL per kg body weight) of physiological saline solution, after ligation of the left lung. The injected volume was inserted and recovered three times, after which the lavage liquid was collected and stored on ice for less than 2 h. To allow necropsy of the planned number of animals within one day, both lungs were lavaged for 10 of the 16 exposed 5xFAD mice and 5 of the 10 exposed C57BL/6J mice, using the same procedure, but approximately 0.8 mL (40 mL per kg body weight) of physiological saline solution. BALF was centrifuged at 400g for 10 min at 4 °C. The supernatant was divided into two separate aliquots of 125 µL for total protein (TP; an indicator for acute lung injury), lactate dehydrogenase (LDH; an indicator of cytotoxicity), gamma-glutamyl transferase (GGT; an indicator of lung cell damage) and alkaline phosphatase (ALP; an indicator of type II cell damage) measurements using an autoanalyser (LX20-Pro; Beckman-Coulter, Woerden, the Netherlands). The cell pellet was scored for the presence of erythrocytes, re-suspended in 500 µL phosphate-buffered saline (PBS) and kept on ice. Cell counts were determined in the re-suspended pellet using a Coulter counter (Beckman-Coulter; Live Sciences, Woerden, the Netherlands). Cell concentrations were determined using a single sample using at least 150 µL of the re-suspended cells. Cytospins (Cytospin 3; Thermo-Shandon, Runcorn, UK) were prepared and stained using May-Grünwald and Giemsa stain, and cell differentiation was performed by counting 400 cells per slide.

Histopathology

Lung tissue. For the majority of the animals, the right lung was removed after the collection of the BALF and immediately frozen in liquid nitrogen and stored at –80 °C for further analysis. The left lung was removed and, after weighing, cannulated and infused with formaldehyde for 1 h at a pressure of 20 cm H₂O. Lungs were processed for histopathology; embedded in paraffin wax, sectioned at a thickness of 2–4 µm and stained with hematoxylin and eosin for histopathological examination. Histopathological changes were described according to distribution, severity and morphological

characteristics. The morphological characteristics of chronic inflammation include for example the presence of lymphocytes and macrophages in the lung tissue, while acute inflammation is characterized by the presence of polymorphonuclear neutrophils (PMNs). Severity scores were assigned as follows: Grade 1 minimal/very few/very small; Grade 2 slight/few/small; Grade 3 moderate/moderate number/moderate size; Grade 4 marked/many/large; Grade 5 massive/extensive number/extensive size.

To allow necropsy of the planned number of animals within one day, both lungs were lavaged for 10 of the 16 exposed 5 × FAD mice and 5 of the 10 exposed C57BL/6J mice. For the remaining six of the 16 exposed 5 × FAD mice both lungs were infused with formaldehyde and embedded in paraffin wax for histopathological examination. For the remaining five of the 10 exposed C57BL/6J mice the right lung was weighed and immediately frozen in liquid nitrogen for determination of the Ce and Zr concentrations and the left lung was infused with formaldehyde and embedded in paraffin wax for histopathological examination. For five of the 10 control C57BL/6J mice the right lung was lavaged and stored at -80°C and the left lung was weighed and immediately frozen in liquid nitrogen for determination of the Ce and Zr concentrations.

Assessment of atherosclerosis. Arteries (brachiocephalic, aortic arch, thoracic aorta) were isolated from $\text{ApoE}^{-/-}$ mice. Atherosclerosis was quantified, as previously published (Miller et al., 2013). Briefly, brachiocephalic arteries were fixed in formalin and histological sections were taken in triplicate at 100 μm intervals, beginning at the first section of the artery with a fully intact media. Sections were stained with Masson's Trichrome. The cross-sectional area of the plaque was measured and standardized to the medial area. A single mean value for atherosclerotic burden for each animal was calculated from the plaque size from each complete serial section throughout the brachiocephalic artery. A single section from each artery (the section exhibiting the largest plaque in cross-section) was chosen for macro-2 immunohistochemistry for macrophage-derived cells. A rat anti-mouse primary antibody was used (1/12000; CL8942AP, VH Bio, Gateshead, UK) with rat IgG (1/12000; I-400, Vector Labs, Peterborough, UK) as a negative control, followed by a goat anti-rat IgG biotinylated secondary antibody (BA-9400; Vector Labs, Peterborough, UK). The area of positive staining was expressed as a proportion of the total plaque area.

Other organs. The spleen, liver, heart and kidneys were removed, weighed and stored in 4% formaldehyde for pathological analysis if required based on macroscopic findings.

Statistical analyzes

Statistical analyzes were performed using GraphPad Prism v7.00 (GraphPad Software, San Diego, CA, USA). Ordinary one-way analysis of variance (ANOVA) analyzes including all experimental groups were performed followed by a Tukey's post-hoc multiple comparisons test. A $p \leq 0.05$ was considered statistically significant. If the group means indicated an increase or decrease with increasing amounts of Zr-doping, a linear trend analysis (alpha 0.1) was performed between the groups exposed to 0%, 27% and 78% Zr-doped CeO_2 NPs, to investigate if observed effects could be related to the amount of Zr doping of the particles.

Results

Nanoparticle characterization

UV-vis analysis showed a clear trend of increasing $\text{Ce}^{3+}/\text{Ce}^{4+}$ ratio with increasing Zr content (see Figure 2 and Table 1). The DCS

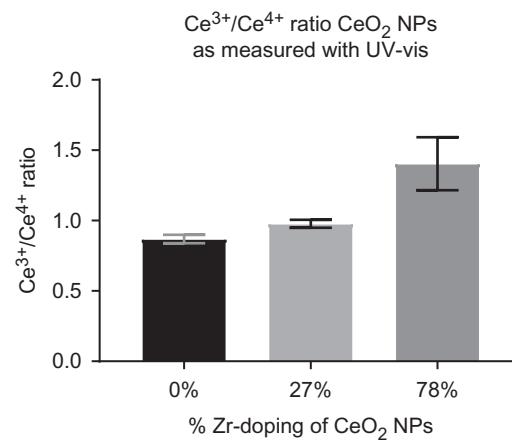


Figure 2. $\text{Ce}^{3+}/\text{Ce}^{4+}$ ratio measured with UV-vis of undoped CeO_2 , 27% Zr-doped CeO_2 and 78% Zr-doped CeO_2 NPs, showing an increasing $\text{Ce}^{3+}/\text{Ce}^{4+}$ ratio with increasing Zr-content of CeO_2 NPs.

ESR measurements of the scavenging capacity of CeO_2 and Zr-doped CeO_2 NPs

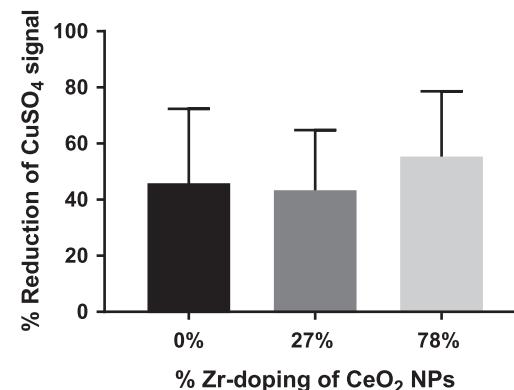


Figure 3. Percentage reduction of the electron-spin resonance (ESR) signal of CuSO_4 and CeO_2 NPs compared to CuSO_4 alone using a cell free system with a 5,5-dimethyl-1-pyrroline N-oxide (DMPO) spin trap in combination with H_2O_2 . The slightly larger % reduction of the 78% Zr-doped NPs indicates a slight but not statistically significant increase in scavenging capacity of reactive oxygen species (ROS) of 78% Zr-doped compared to the undoped and 27% Zr-doped CeO_2 NPs.

and DLS analysis both showed no significant differences in hydrodynamic size distributions (data not shown) or median particles size (see Table 1) of the different NPs, indicating the Zr-doping did not cause major differences in particle size distribution, aggregation or agglomeration. As expected, the zeta potential showed a small decrease with increasing amounts of Zr-doping.

Electron-spin resonance analysis showed a slight, but not statistically significant increased scavenging capacity of the CeO_2 NPs with the highest % of Zr-doping compared to the undoped CeO_2 NPs (see Figure 3 and Table 1).

In A549 cells, a decrease in cytotoxicity with increasing amounts of Zr-doping was shown. Dose response modeling resulted in increasing EC_{20} values with increasing amounts of Zr-doping (see Figure 4 and Table 1).

Exposure characterization

The combined SMPS-OPS particle size measurements showed that almost the entire particle size distribution was within the size range measurable with the SMPS (2.5–1000 nm), confirming that the SMPS data can be used to estimate the CMD and MMD.

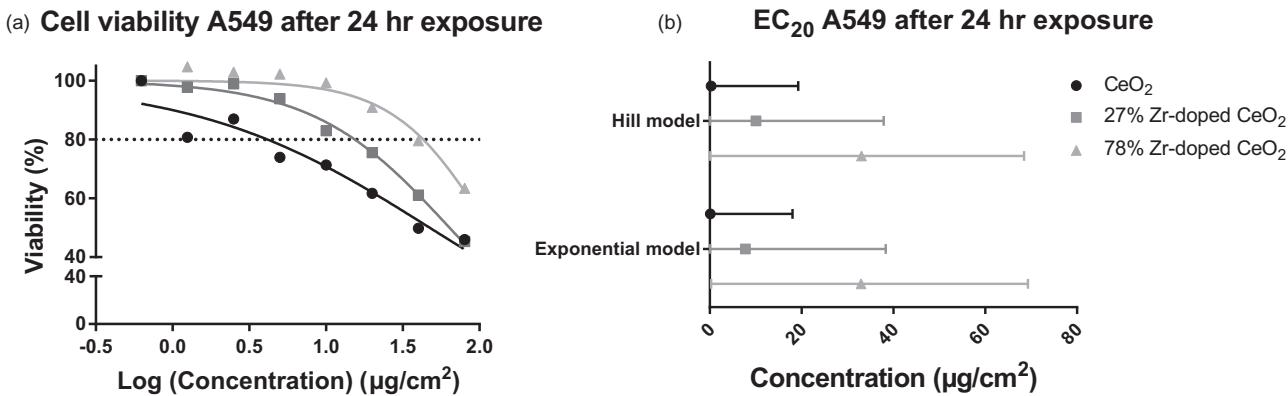


Figure 4. Percentage reduction in viability of A549 cells after exposure to 0, 1.25, 2.5, 5, 10, 20, 40 or 80 $\mu\text{g}/\text{cm}^2$ CeO₂, 27% Zr-doped CeO₂ and 78% Zr-doped CeO₂ NPs compared to the controls (a) and the effective concentrations resulting in 20% cytotoxicity (EC₂₀) mean \pm 90% confidence interval (b).

A representative SMPS and OPS size distribution of each of the different CeO₂ NPs are shown in Figure 5.

The physical characteristics of the different CeO₂ NP aerosols are summarized in Table 2. The primary particle size of the different CeO₂ NPs was $\sim 4.7 \pm 1.4$ nm. CMD and MMD, as measured by SMPS, were slightly larger for the 78% Zr-doped CeO₂ particles, compared to the CeO₂ and 27% Zr-doped CeO₂ particles. Mass concentration measurements determined the exposure concentration, thus, the particle number concentrations of the 78% Zr-doped CeO₂ exposure were lower than the particle number concentrations of the CeO₂ and 27% Zr-doped CeO₂ exposures.

Scanning electron microscopy images of the NPs from aerosols collected on polycarbonate filters showed the presence of particles and agglomerates, when collected on the filter (see Figure 6). Most particles were around 300–500 nm, but there were also infrequent very large particles (around 1000–2000 nm).

Estimated deposited dose in lungs

The estimated deposited dose in the lung and head was similar for CeO₂, 27% Zr-doped CeO₂ and 78% Zr-doped CeO₂ NPs, ranging from 618 to 639 ng (approximately 60% of the inhaled dose). The deposition pattern in the different regions of the lungs was also similar for the different types of CeO₂ NPs, with approximately 8% of the dose reaching the alveoli (see Table 3).

Quantification of Ce and Zr in tissues

The highest concentrations of Ce and Zr were found in the lung, followed by much lower concentrations in the heart, spleen, kidneys and liver, respectively (Figure 7). As would be expected, significantly higher levels of Ce and Zr were observed in the lungs of exposed mice compared to the controls. Increasing amounts of Zr-doping in the NP exposure did not result in decreasing Ce concentrations or increasing Zr concentrations in the lung. In most of the other organs, the Ce and Zr concentrations were not statistically significantly different from the background concentrations measured in the controls. A few exceptions were observed, for example, the Ce concentration in the hearts of mice exposed to 78% Zr-doped CeO₂.

Hematology

ApoE^{-/-} mice had more neutrophils compared to exposed and control C57BL/6J and 5 × FAD mice ($p < 0.05$ in Tukey's post-hoc test following one-way ANOVA). No statistically significant differences were observed in the total white blood cell counts

(data not shown) or differential white blood cell counts (Figure 8) of the exposed groups compared to the controls in blood from all strains of mice, except for a small decrease in neutrophils in ApoE^{-/-} mice exposed to 78%-doped CeO₂ NPs (Tukey's post-hoc test following one-way ANOVA with $p = 0.02$). In addition, there was a decrease (post-hoc test for linear trend following one-way ANOVA with $p = 0.002$) in neutrophils in ApoE^{-/-} mice with increasing amounts of Zr-doping.

Bronchoalveolar lavage

The number of lymphocytes in the control C57BL/6J mice was relatively high (7.7%), but this was due to an outlier and did not represent an inflammatory response. No statistically significant differences were observed in the total cell counts (data not shown) or differential cell counts in BALF of the exposed groups compared to the controls for any strain of mouse (Figure 9), except for the total cell count in 5 × FAD mice exposed to 27% Zr-doped CeO₂ NPs, which was lower than that of the control 5 × FAD mice. There was a decrease ($p < 0.1$; post-hoc test for linear trend following one-way ANOVA) in total cell counts ($p = 0.075$), % macrophages ($p = 0.014$), and % neutrophils ($p = 0.05$) in ApoE^{-/-} mice with increasing amounts of Zr-doping. However, no such trends were observed in C57BL/6J or 5 × FAD mice. Similarly, no statistically significant differences were observed for LDH, ALP or GGT protein levels between the exposed and control groups (Figure 10). No constitutive differences in differential cell counts or protein levels were observed between the different mice strains.

Histopathology

Lung

While modest, an increased incidence in minimal chronic bronchoalveolar or alveolar inflammation was observed in the exposed animals compared to the control mice (see Figure 11(a–c)). The increase did not appear to be related to the percentage Zr-doping (Table 4).

Particle-loaded alveolar macrophages (Figure 11(e)) were observed in seven of the eight ApoE^{-/-} mice exposed to undoped CeO₂ NPs. This effect was not observed in ApoE^{-/-} mice exposed to 27% or 78% Zr-doped CeO₂ NPs or any other exposure or the control group of the other mouse models (Table 4), indicating Zr-doping may influence particle loading of alveolar macrophages in ApoE^{-/-} mice. In the bronchoalveolar lavage fluid

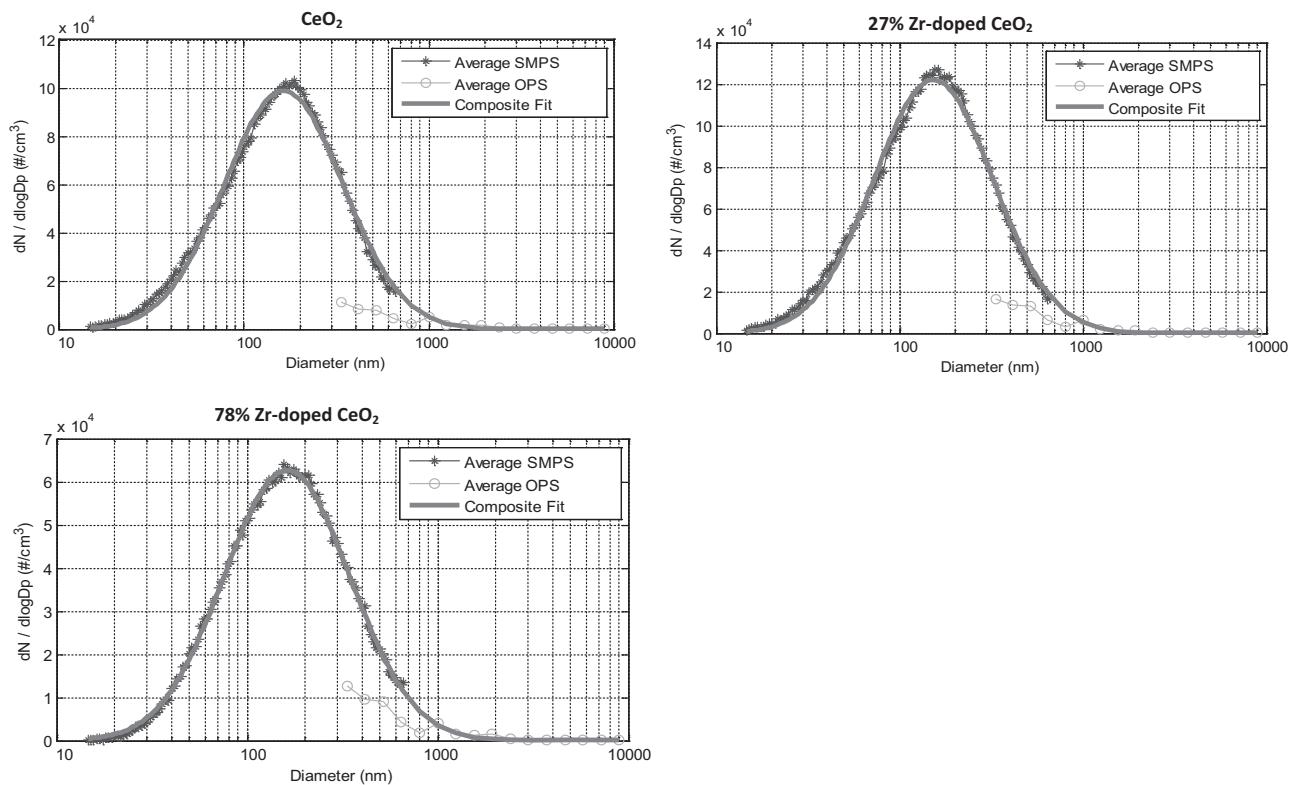


Figure 5. Combined size distributions measured with the scanning mobility particle sizer (SMPS) and the optical particle sizer (OPS) for representative samples of CeO_2 , 27% Zr-doped CeO_2 and 78% Zr-doped CeO_2 NPs. The OPS distributions overlap with the composited fit of the SMPS distributions for the largest particles of the distributions, indicating that the SMPS measurements can be used to determine the count median diameter (CMD) and mass median diameter (MMD).

particle-loaded macrophages were seen in all the NP exposed animals but not in the control groups.

Cardiovascular effects

$\text{ApoE}^{-/-}$ mice exhibited regions of dense plaques in the aortic arch and branch points of large arteries. Plaques were composed of fibroblastic matrix, smooth muscle cells, lipid cavities and cholesterol crystals (Figure 12(a)). Atherosclerotic burden was quantified in the brachiocephalic artery, with control (air-exposed) mice having a mean plaque size of $94 \pm 9\%$ (standardized to the area of the vascular media). Exposure to undoped or Zr-doped CeO_2 NPs did not have a significant effect on the atherosclerotic burden (mean plaque size) of these arteries ($p = 0.62$; one-way ANOVA; Figure 12(b)). However, there was an increase (post-hoc test for linear trend following one-way ANOVA with $p = 0.09$) in the proportion of plaque staining positive for mac-2 (i.e. macrophage-derived foam cells; Figure 12(c)) with increasing Zr content of the CeO_2 NP exposure (Figure 12(d)).

Other organs

No treatment related effects on organ weights or macroscopic findings (data not shown) were observed and thus no histopathological analysis was performed on the other organs.

Discussion

In this subacute inhalation study, only modest biological effects were observed after exposure to CeO_2 NPs or Zr-doped CeO_2 NPs in healthy mice and mouse models of atherosclerosis and Alzheimer's disease. Accordingly, altering the redox activity of nanomaterials by Zr-doping had a limited impact on the bioactivity, in the absence of any overt toxicity of the CeO_2 parent material.

Zr-doping of CeO_2 NPs

Zr-doping of CeO_2 NPs was expected to increase the antioxidant potential of CeO_2 NPs by shifting the Ce valence state towards 3^+ , increasing its capacity to shift from 3^+ to 4^+ and thus increasing its antioxidant potential and thereby reducing adverse pulmonary and cardiovascular effects. Our UV-vis analyzes confirmed that Zr-doping does shift the valence state towards 3^+ (see Figure 2). Furthermore, ESR analysis using a DMPO spin trap in combination with H_2O_2 showed that high concentrations of Zr-doping increased the scavenging capacity for ROS by CeO_2 NPs in a cell-free system (see Figure 3). In addition, *in vitro* tests indicated that Zr-doping decreased the cytotoxicity of CeO_2 NPs in human alveolar cells (A549) (see Figure 4). However, *in vivo* Zr-doping had a limited impact on the pulmonary and cardiovascular effects.

Previous studies investigated the effect of samarium (Sm) or gadolinium (Gd) doping of CeO_2 NPs (Celardo et al., 2011; Dunnick et al., 2015, 2016). Sm-doping decreased the $\text{Ce}^{3+}/\text{Ce}^{4+}$ ratio and thereby the ability to shift from 3^+ to 4^+ , decreasing the antioxidant properties of CeO_2 NPs in leukocyte (U937 and Jurkat) cell lines (Celardo et al., 2011). Gd-doping increased the $\text{Ce}^{3+}/\text{Ce}^{4+}$ ratio, but also decreased the ability to shift from 3^+ to 4^+ and the antioxidant properties, suggesting that differences in reactivity of CeO_2 NPs are due to the ability of Ce to transition between the two valence states rather than dependent on a specific valence state (Dunnick et al., 2015, 2016). Although Zr-doping increased the $\text{Ce}^{3+}/\text{Ce}^{4+}$ ratio of the CeO_2 NPs, the ability to shift from 3^+ to 4^+ may be reduced instead of enhanced due to Zr-doping, because the Zr-atoms occupy some of the 4^+ sites.

In addition, the antioxidant activity of CeO_2 NPs can also be affected by the external environment, especially the anions (Xue et al., 2012). Xue et al. (2012) showed that CeO_2 NPs scavenge hydroxyl radicals ($\cdot\text{OH}$) in Tris hydrochloride (Tris-HCl) and sulfate

Table 2. Average particle number concentration, size distribution and mass concentration of the CeO_2 , 27% Zr-doped CeO_2 and 78% Zr-doped CeO_2 NP exposure ($n = 20$).

			CeO_2	27% Zr-doped CeO_2	78% Zr-doped CeO_2
STEM	Primary particle size ^a	nm	4.7 \pm 1.4	4.6 \pm 1.4	4.7 \pm 1.4
CPC	Number concentration	#/ cm^3	14,624 \pm 3709	16,962 \pm 5145	10,785 \pm 894
SMPS	Count median diameter (CMD)	nm	182 \pm 10	183 \pm 9	202 \pm 7
	Geometric standard deviation		1.88	1.88	1.86
	Mass median diameter (MMD) ^b	nm	280 \pm 12	288 \pm 9	316 \pm 14
	Geometric standard deviation		1.55	1.56	1.57
Filter	Number concentration	#/ cm^3	75,620 \pm 28,184	70,828 \pm 46,924	58,716 \pm 20,693
	Gravimetric mass concentration	mg/ m^3	3.98 \pm 0.23	4.04 \pm 0.30	4.09 \pm 0.22

^aPrimary particle size was determined by scanning transmission electron microscope (STEM) electron energy loss spectroscopy (EELS) analysis.

^bMMD was estimated based on the particle size distributions of the SMPS measurements, assuming spherical aggregation around primary particles of 4.7 nm.

All values are means \pm standard deviation.

CPC: condensation particle counter; SMPS: scanning mobility particle sizer.

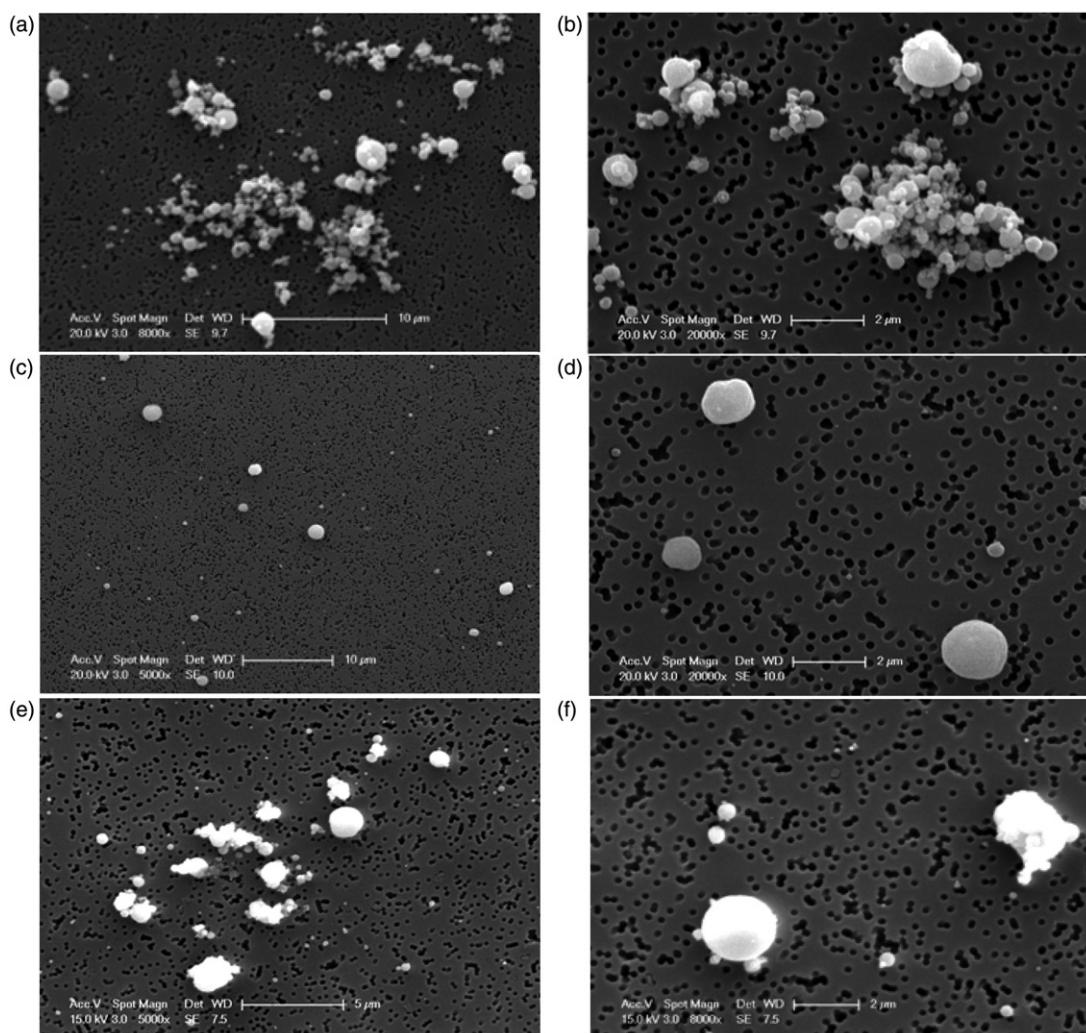


Figure 6. Scanning electron microscopy (SEM) image of CeO_2 particles from aerosols collected on polycarbonate filters. Undoped CeO_2 NPs (a and b) showed the presence of agglomerates mostly around 300 to 400 nm, but also some infrequent very large particles around 2000 nm. About 27% Zr-doped CeO_2 NPs (c and d) showed no agglomerates and particles were mostly around 500 nm. About 78% Zr-doped CeO_2 NPs showed the presence of agglomerates, mostly around 400 nm, but also some very large particles around 1000 nm and a significant amount of smaller particles of approximately 200 nm or smaller (e and f).

systems, but lose their scavenging capacity in PBS. Their explanation for this is that the antioxidant activity of CeO_2 NPs is not only determined by its ability to convert Ce^{3+} into Ce^{4+} , but also by regeneration of Ce^{3+} by reduction of Ce^{4+} on the surface of the nanoparticles. According to Xue et al. (2012) in PBS cerium phosphate is formed on the surface of the NPs, which prevents the regeneration of Ce^{3+} from Ce^{4+} during the redox cycling preventing the CeO_2 NPs to scavenge $\cdot\text{OH}$. Although the aerosols of

the Zr-doped CeO_2 NPs were prepared using ultrapure water instead of PBS, the antioxidant potential of the CeO_2 NPs may be similarly altered once deposited in the lungs of the mice.

Particle deposition and distribution to other organs

The deposition along different regions of the respiratory tract of mice, calculated with the MPPD model (v3.04), was similar for the

Table 3. Estimated deposition of inhaled CeO₂, 27% Zr-doped CeO₂ and 78% Zr-doped CeO₂ NPs in different regions of the lungs.

	Total inhaled dose (µg) ^a	Total deposited dose (µg) ^b	Deposited fraction per region (% of inhaled dose) ^b			
			Head (%)	Tracheobronchial region (%)	Alveolar region (%)	
CeO ₂ NPs	1027	618	48.8	3.5	8.0	16.2
27% Zr-doped CeO ₂ NPs	1043	625	48.8	3.4	7.9	16.2
75% Zr-doped CeO ₂ NPs	1056	639	49.8	3.3	7.5	15.6

^aTotal amount inhaled = estimated as tidal volume (0.203 mL) × breathing frequency (353 min⁻¹) × exposure concentration ($\approx 4 \times 10^{-3}$ µg/mL) × exposure duration (3600 min).

^bEstimated using the MPPD model.

^cRetained dose in the tracheobronchial and alveolar region four weeks post-exposure, estimated using the MPPD model.

Ce and Zr concentrations in different organs

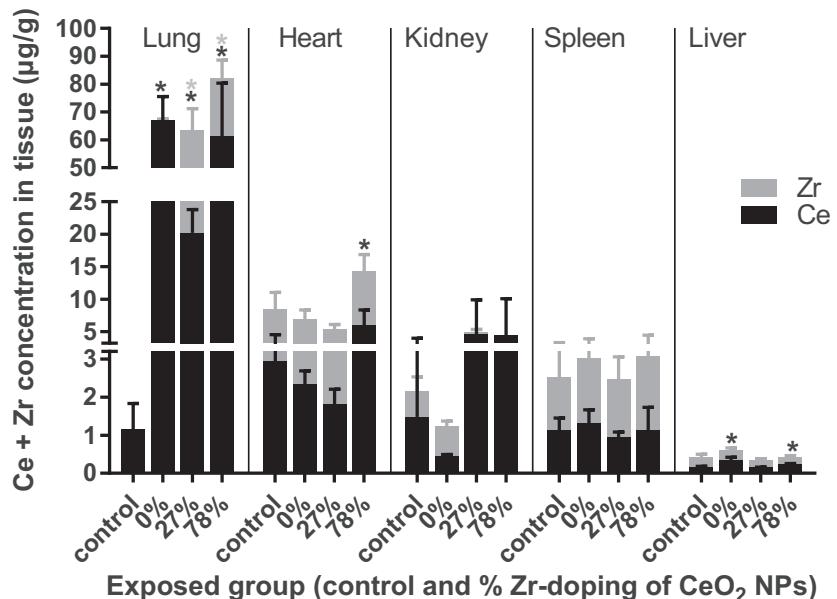


Figure 7. Ce and Zr concentrations in organs 4 weeks after exposure to clean air (control) or 0%, 27% or 78% Zr-doped CeO₂ NPs (exposed). Mean \pm SD, $n = 4-6$. *—Ce or Zr concentration is statistically significantly different from the control in Tukey's post-hoc test following one-way ANOVA with $p < 0.05$. The bar graphs are stacked and represent the sum of the Ce concentration (bottom black colored part of each bar) and Zr concentration (upper gray colored part of each bar) in the different organs. With a few exceptions (e.g. the lung), the Ce and Zr concentrations of the exposed animals were not statistically significantly different from the control animals in most organs. The Zr concentration in the lungs of the control group and in the kidneys of the group exposed to 78% Zr-doped CeO₂ NPs was below the detection limit.

different types of undoped and Zr-doped CeO₂ NPs. In all cases, the estimated fraction of particle deposition in the lung (tracheobronchial and alveolar region) was approximately 11% of the inhaled mass dose.

As expected, the highest cerium (Ce) and zirconium (Zr) concentrations, as measured by ICP-MS analysis of tissues, were found in the lung. The MPPD model can be used to predict the Ce dose in the lung four weeks post-exposure if it is assumed there is an even distribution of the CeO₂ NPs in the lungs. Based on the estimated retained dose of CeO₂ NPs (with 0% Zr-doping) in the lung (16.2 µg, see Table 3) and the average lung weight (158 mg), the expected Ce concentration in the lung is approximately 103 µg/g. The measured Ce concentration in the right lungs of the undoped CeO₂ NP exposed mice was slightly lower (67 µg/g) but in the same order of magnitude. The difference between the predicted and measured concentrations may reflect the lung clearance rate used by the MPPD model compared to the actual lung clearance rate *in vivo*.

Background levels of Ce and Zr were detected in various organs of animals exposed to clean air (controls). This might be caused by Ce and Zr contamination of the drinking water, food and/or bedding of the animals. Although Ce and Zr

concentrations are not routinely measured in drinking water, food or bedding, Ce was detected in rat chow in a concentration of 0.22 mg Ce/kg food (Yokel et al., 2012) and in tap water in concentrations of ~ 0.0009 µg/L in the US (Donovan et al., 2016) and 0.018–0.084 µg/L in Croatia (Fiket et al., 2015). In addition, Ce has been detected in various organs of control animals in previous *in vivo* studies (Yokel et al., 2012, 2013).

The Ce and Zr concentrations in the lung did not reflect the different percentages of Zr-doping of the NPs, as would have been expected. Increasing amounts of Zr-doping did not lead to higher Zr concentrations or lower Ce concentrations. Moreover, surprisingly low Ce concentrations were found in the lungs of mice exposed to 27% Zr-doped CeO₂ NPs compared to mice exposed to 78% Zr-doped CeO₂. These findings are unlikely to be due to the differences in exposure or deposition of the NPs, since the gravimetric mass concentrations and size distribution of the aerosols were almost identical (Table 2). These unexpected findings might reflect differences in clearance, de-agglomeration or dissolution of the different CeO₂ NPs types in the lung, based on, for example, differences in agglomeration size and surface specific uptake by macrophages. We speculate that Zr-doping may increase the clearance of the NPs, since a previous study showed

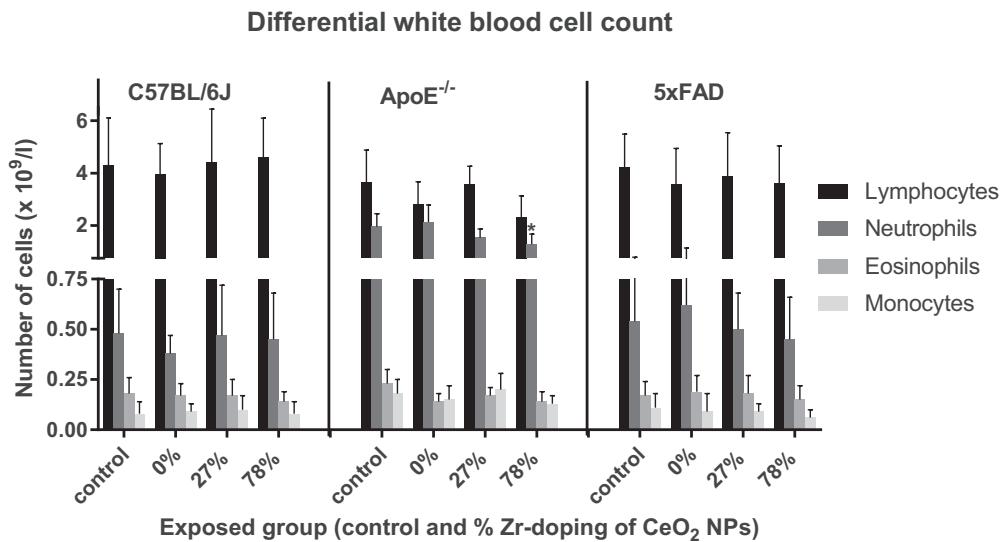


Figure 8. Differential white blood cell count four weeks after exposure to clean air (control) or 0%, 27% or 78% Zr-doped CeO_2 NPs (exposed). Mean \pm SD, $n = 8-16$, * = statistical significantly different from the control in Tukey's post-hoc test following one-way ANOVA with $p < 0.05$. No statistically significant differences between the different types of white blood cells were observed between control and exposed animals, except for the neutrophils in $\text{ApoE}^{-/-}$ mice exposed to 78% Zr-doped CeO_2 NPs. The number of basophils and large unstained cells were very small and are thus not depicted.

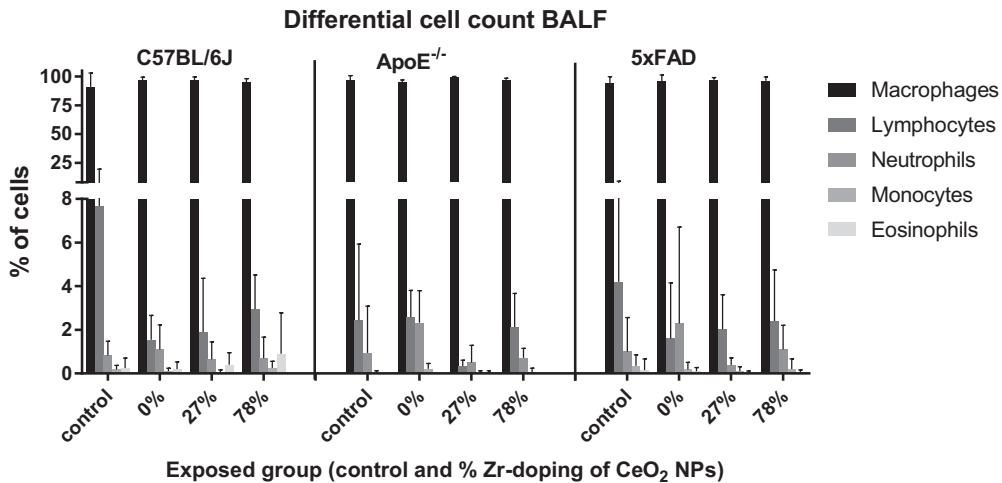


Figure 9. Differential cell count in bronchoalveolar lavage fluid (BALF) 4 weeks after exposure to clean air (control) or CeO_2 , 27% Zr-doped CeO_2 or 78% Zr-doped CeO_2 NPs (exposed). Mean \pm SD, $n = 5-16$, * = statistical significantly different from the control in Tukey's post-hoc test following one-way ANOVA with $p < 0.05$. No statistically significant differences in the different types of cells were observed between control and exposed animals, except for the number of macrophages in 5 \times FAD mice exposed to 27% Zr-doped CeO_2 NPs.

that the decrease in lung burden during the post-exposure period of 21 days was markedly higher for ZrO_2 NPs (42–75% decrease) compared to CeO_2 NPs (5–7% decrease) (Landsiedel et al., 2014). Alternatively, it is possible that the particles may have had different effective densities that might have affected the distribution pattern.

The concentrations of Ce and Zr in heart, spleen, kidneys and liver were much lower than what was measured in the lung. Similar distribution patterns have been found in other studies after inhalation of CeO_2 NPs (Aalapati et al., 2014; Geraets et al., 2012; Keller et al., 2014).

Pulmonary effects

CeO_2 NP exposure had no statistically significant effects on total and differential cell counts, LDH, ALP, GGT or total protein levels in the BALF of any of the tested mouse strains four weeks post-exposure, irrespective the Zr content. Only modest inflammatory

lesions were found by histopathological analysis of lung sections of CeO_2 NPs exposed mice. As these findings were not related to the amount of Zr-doping, the observed pulmonary effects are likely to be caused by the physical interaction between the alveolar surface and the large reactive surface area of the particles, an observation not uncommon with poorly-soluble nanoparticles (Greim & Ziegler-Skylakakis, 2007). One exception to these findings were the particle-loaded alveolar macrophages in histological lung sections of $\text{ApoE}^{-/-}$ mice that were only observed after exposure to CeO_2 NPs without Zr-doping, indicating Zr-doping may influence the occurrence of particle-loaded alveolar macrophages. Interestingly, in the BALF, particle-loaded macrophages were seen in all the exposed groups (all mouse models and all CeO_2 NP types). This observation might reflect differences in the dynamics of macrophages of the $\text{ApoE}^{-/-}$ mice; for example the inherently higher number of macrophages in the lungs of this strain of mouse (Grainger et al., 2004), which can be further increased by a high fat diet (Naura et al., 2009). Differences in the ability of the

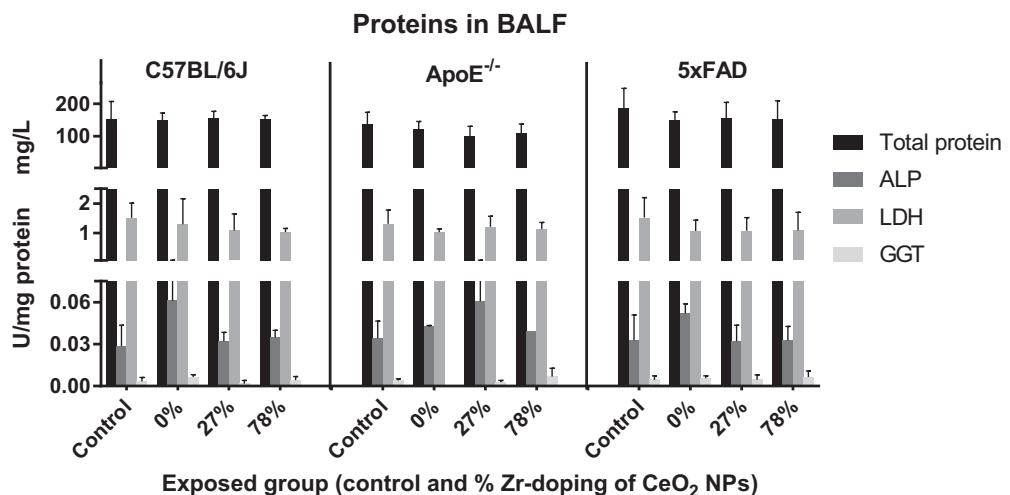


Figure 10. Total protein, lactate dehydrogenase (LDH), alkaline phosphatase (ALP) and gamma-glutamyl transpeptidase (GGT) levels in bronchoalveolar lavage fluid (BALF) four weeks after exposure to clean air (control) or CeO₂ and 27% Zr-doped CeO₂ or 78% Zr-doped CeO₂ NPs (exposed). Mean \pm SD, $n = 5-16$. No statistically significant differences in the total protein, LDH, ALP or GGT were observed between control and exposed animals (Tukey's post-hoc test following one-way ANOVA with $p < 0.05$).

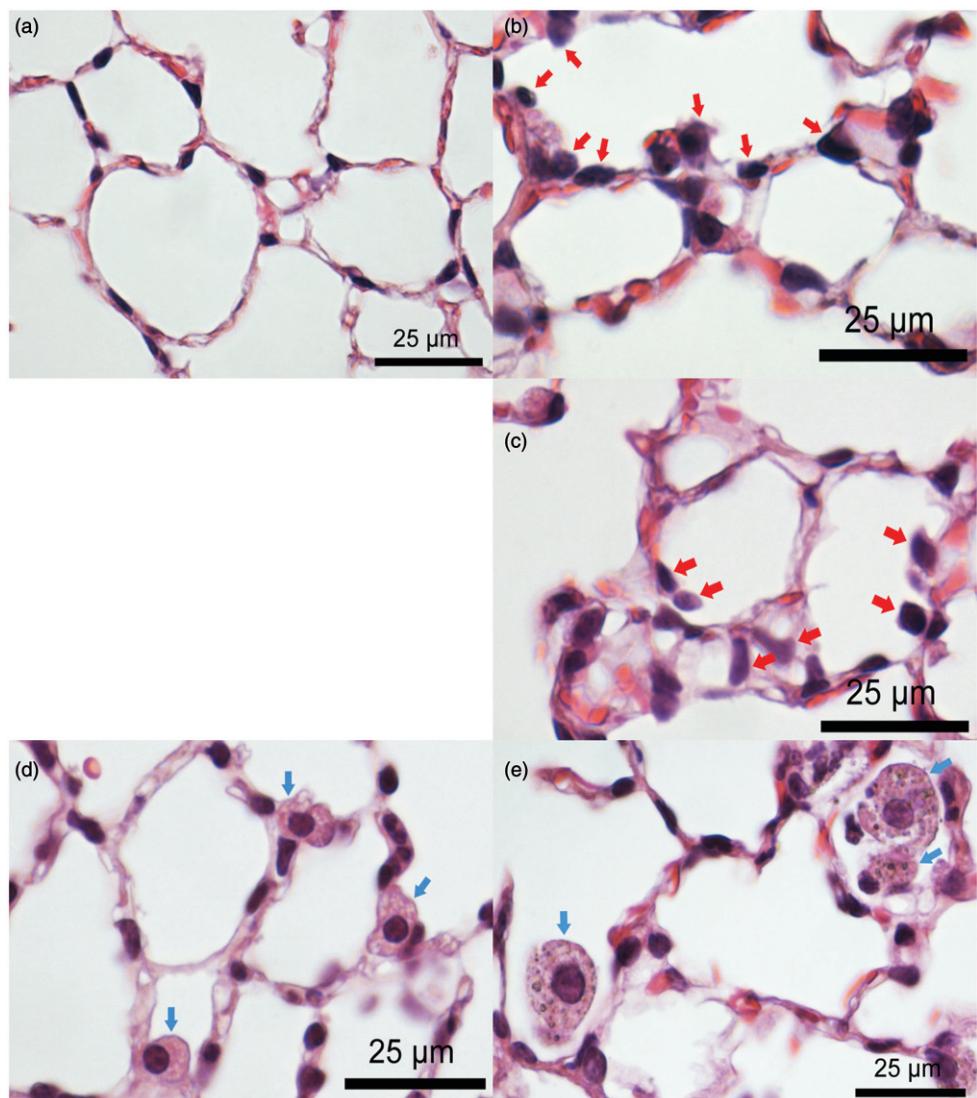


Figure 11. Lung sections showing minimal chronic bronchoalveolar inflammation, alveolar inflammation and particle-loaded alveolar macrophages in mice exposed to doped and undoped CeO₂ NP exposure. Lung sections of C57BL/6J mice exposed to clean air (a) and 78% Zr-doped CeO₂ NPs (b and c) and of ApoE^{-/-} mice exposed to 27% Zr-doped CeO₂ NPs (d) and undoped CeO₂ NPs (e). Red arrows indicate mononuclear inflammatory cells on the septa of the alveoli, indicating minimal chronic bronchoalveolar inflammation (b) or inside the alveoli, indicating minimal alveolar inflammation (c). Lung sections of mice with chronic and alveolar inflammation were similar across the different mouse models and experimental groups. Blue arrows indicate empty (d) or particle-loaded (e) alveolar macrophages.

Table 4. Histopathological findings in lung of C57BL/6J, ApoE^{-/-} and 5xFAD mice.

Histopathological finding →		Chronic bronchoalveolar or alveolar inflammation		Alveolar macrophages	Particle-loaded alveolar macrophages	
Strain ↓	Treatment ↓	Minimal	Slight		Minimal	Slight
C57BL/6J	Control	60% (3/5) ^a	–	–	–	–
	Total exposed	67% (10/15)	–	13% (2/15)	–	–
	CeO ₂	80% (4/5)	–	20% (1/5)	–	–
	27% Zr-doped CeO ₂	40% (2/5)	–	20% (1/5)	–	–
	78% Zr-doped CeO ₂	80% (4/5)	–	–	–	–
	Control	25% (2/8)	–	–	–	–
	Total exposed	42% (10/24)	–	–	4% (1/24)	25% (6/24)
	CeO ₂	38% (3/8)	–	–	13% (1/8)	75% (6/8)
ApoE ^{-/-}	27% Zr-doped CeO ₂	38% (3/8)	13% (1/8)	–	–	–
	78% Zr-doped CeO ₂	50% (4/8)	–	–	–	–
	Control	69% (11/16)	–	6% (1/16)	–	–
	Total exposed	72% (13/18)	–	17% (3/18)	–	–
	CeO ₂	83% (5/6)	–	17% (1/6)	–	–
	27% Zr-doped CeO ₂	67% (4/6)	–	–	–	–
	78% Zr-doped CeO ₂	67% (4/6)	–	33% (2/6)	–	–

^aPercentage of animals affected. Within brackets the number of animals with histopathological findings versus number of animals evaluated.

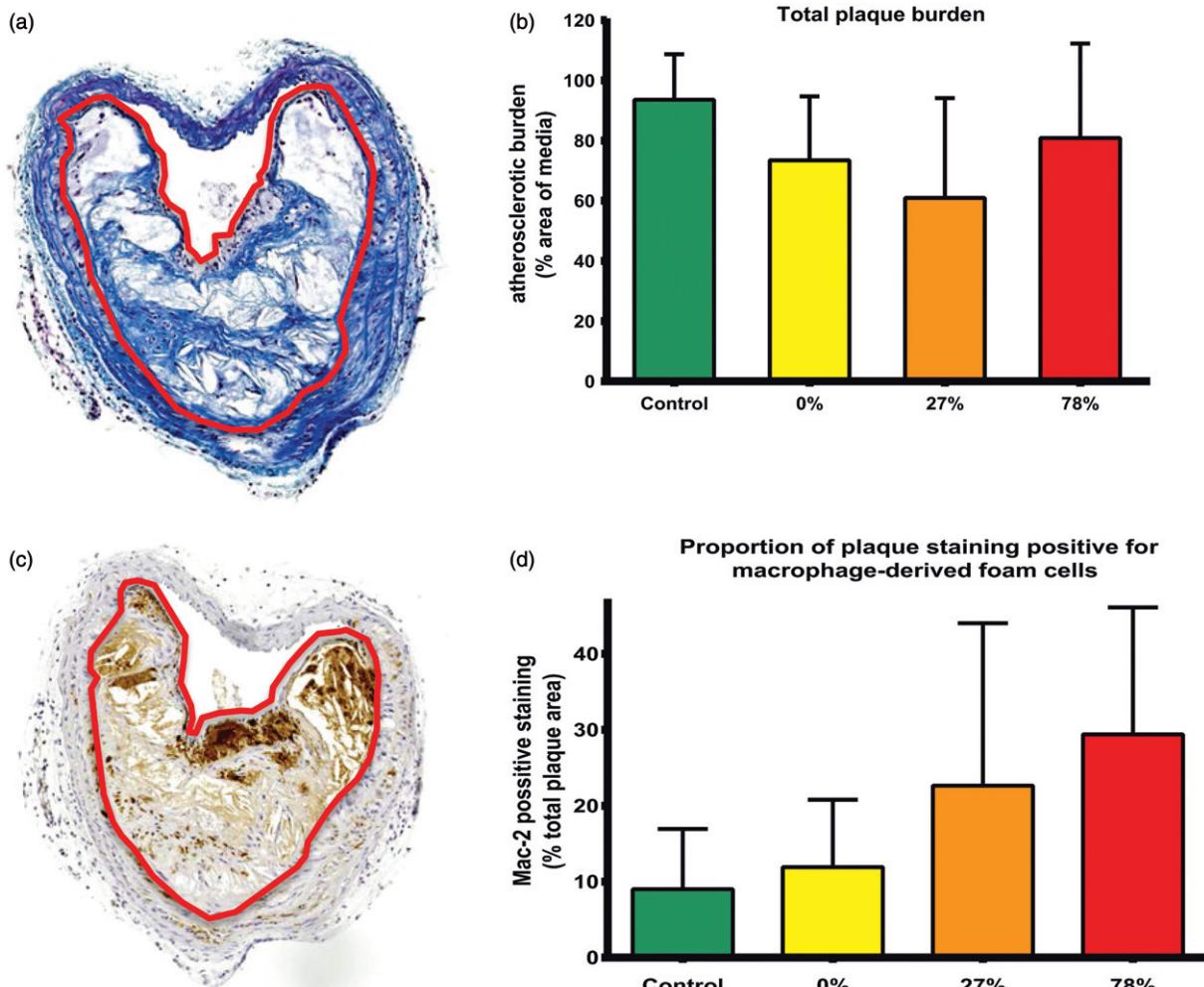


Figure 12. Effect of Zr-doped CeO₂ NPs on atherosclerosis in the brachiocephalic artery of ApoE^{-/-} mice after inhalation. (a) Representative section of brachiocephalic artery showing a large plaque on the intimal surface of the artery. The red outline highlights the area of the plaque. (b) Quantification of atherosclerotic burden throughout the brachiocephalic artery. Mean ± SEM ($n = 3-7$). Undoped (0%) or Zr-doped (27% and 78%) CeO₂ NP exposure did not significantly affect plaque size compared to clean air exposure (controls). (c) Immunohistochemical staining for mac-2 (brown stain, showing macrophage-derived foam cells). The red outline highlights the area of the plaque. (d) Proportion of plaque staining positive for mac-2 following exposure to clean air (control), undoped (0%) and Zr-doped (27% and 78%) CeO₂ NPs. Mean ± SEM ($n = 4-7$). No statistically significant differences were observed between control and exposed animals (Tukey's post-hoc test, following one-way ANOVA with $p < 0.05$). Scale bars = 100 μ m.

undoped and the Zr-doped CeO_2 NP types to influence the NP uptake, damage and turnover of macrophages in the lung may result in differences in the release of the NPs from macrophages in the lung, resulting in the observed Zr-doping related differences in the occurrence of particle-loaded alveolar macrophages in the histological lung sections four weeks post-exposure.

Other inhalation studies have reported more prominent effects of CeO_2 NPs than those observed in our study, including increased neutrophils and lymphocytes in BALF, increased concentrations of biochemical markers of inflammation in BALF (LDH, ALP, GGT, *N*-acetyl beta-D-glucosaminidase (NAG) and cytokine-induced neutrophil chemoattractant-1(CINC-1)), increased lung weight, inflammatory lung lesions (e.g. severe alveolitis, particle-loaded macrophages and granulomas, lung fibrosis) and accumulation of particle-loaded macrophages in lymph nodes and liver (Aalapati et al., 2014; Demokritou et al., 2013; Gosens et al., 2014; Keller et al., 2014; Srinivas et al., 2011) (see Tables S1). It is notable that most of these studies were performed in rats, which tend to be more susceptible to pulmonary inflammation induced by poorly soluble particles than mice (Borm et al., 2015). Some of the effects observed in previous studies only occurred at higher exposure concentrations (e.g., 5, 10, 25 or 50 mg/m³ for 6 h/day, 5 d/w for four weeks), compared to the exposure of 4 mg/m³ for 3 h/day, 5d/w for four weeks we used in our study. Additionally, our study focused on the presence of persistent toxicity four weeks post-exposure, when inflammation induced directly after exposure will have gradually diminished to a level that does not manifest in the BALF or histopathology. The prolonged recovery time in our study provides an opportunity to assess whether the biological effects lead to persistent adverse outcomes. Nevertheless, we acknowledge that several prior studies have demonstrated long-lasting pulmonary effects, including raised neutrophils and lymphocytes in BALF and accumulation of particle-loaded macrophages and granulomas in the lung (Aalapati et al., 2014; Keller et al., 2014; Morimoto et al., 2015). A four-week inhalation exposure to similar levels of CeO_2 NPs in CD-1 mice caused inflammation-induced responses in the lung characterized by necrosis, fibrosis and granulomas four weeks post-exposure (Aalapati et al., 2014). Differences in the CeO_2 NPs and exposure characteristics could explain these diverging results. In our study, CeO_2 NPs were produced by hydrothermal synthesis, with primary particle size of ~4.7 nm, and aerosols with a mass median diameter (MMD) of 280 nm with a geometric standard deviation (GSD) of 1.56. Aalapati et al. (2014) used CeO_2 NPs produced via the sol-gel method, with a primary diameter of 15–30 nm and aerosols with a mass median aerodynamic diameter (MMAD) of 1.4 μm (GSD 2.4). Both the cumulative external dose, (i.e. concentration \times exposure duration) and the dose rate were very similar for both studies, however, differences in particle size distribution will have led to different biological effective pulmonary doses. The measured Ce concentration in the lung four weeks post-exposure reported by Aalipati et al. was much higher (approximately 500 $\mu\text{g/g}$ tissue compared to 67 $\mu\text{g/g}$ in our study). The higher Ce concentration is likely to have contributed to the greater pulmonary toxicity in the Aalapati study. Other possible explanations are that CeO_2 NPs generated via sol-gel method have a different redox activity, surface structure or other properties that make them more toxic than CeO_2 NPs generated by hydrothermal synthesis. Furthermore, the strain (CD-1 mice), gender (male) and/or age (7–8 weeks) of the mice used by Aalapati et al. might be more sensitive to the effects of particle inhalation than the strain

(C57BL/6J mice), gender (female) and/or age (nine weeks) of the mice used in our study.

The modest inflammatory lung lesions observed in this study were not related to the amount of Zr-doping of the CeO_2 NPs, with the exception of the particle-loaded alveolar macrophages in histological lung sections of $\text{ApoE}^{-/-}$ mice that were only observed after exposure to CeO_2 NPs without Zr-doping. Recently, another *in vivo* study (Dunnick et al., 2016) investigated the influence of Gd-doping of CeO_2 NPs after inhalation exposure. In this study, Sprague–Dawley rats were exposed to 0.5 or 1.0 mg/kg pure CeO_2 NPs and 10 or 20% Gd-doped CeO_2 NPs via intratracheal instillation. Gd-doping was expected to increase the pulmonary toxicity, but no major effect of doping on the pulmonary toxicity was observed 1, 7 and 84 days after exposure of CeO_2 NPs in rats. Our study used a post-exposure period of four weeks and an exposure concentration that caused pronounced pulmonary toxicity in a previous study (Aalapati et al., 2014). However, because only minimal pulmonary effects were observed after exposure to the CeO_2 NPs without Zr-doping in our study, most of the hypothesized ameliorative effects resulting from the Zr-doping may not have been visible under the present conditions.

Cardiovascular effects

There was no significant effect of CeO_2 NP exposure, or of the Zr-doped variants, on atherosclerotic burden. Previous studies using this mouse model showed that pulmonary exposure to nano-sized carbon black (Niwa et al., 2007), carbon nanotubes (Cao et al., 2014; Li et al., 2007), nickel nanoparticles (Kang et al., 2011) and nano-titanium dioxide (Chen et al., 2013; Mikkelsen et al., 2011) promoted the development of atherosclerosis. There is also a large body of literature showing that inhalation of ultrafine particles in air pollution promotes atherosclerosis in man (Kunzli et al., 2011) and animal models (Miller et al., 2013; Moller et al., 2011). Environmental nanoparticles have a very varied composition, however, the ability of chemicals and metals on the particle surface to generate reactive oxygen species is believed to be a key determinant of their ability to induce cardiovascular effects (Miller et al., 2012). Thus, we envisioned that inhalation of nanomaterials with different amounts of Zr-doping would also induce varying degrees of cardiovascular dysfunction. The lack of effect of Zr-doping of CeO_2 NPs may reflect the low reactivity of the parent compound, or potentially the small degree of deposition in the alveoli, leading to limited lung inflammation or particle translocation to the bloodstream. Interestingly, though, the composition of atherosclerotic plaques tended to be altered by subacute exposure to CeO_2 NPs with increasing Zr content. In particular, there was an increase in the plaque content of macrophage-derived foam cells with an increased proportion of Zr in the CeO_2 NPs. In man, plaques with a greater degree of inflammation are more instable and prone to rupture; the result of which can lead to thrombotic occlusion of the vessel causing a cardiovascular event, e.g. heart attack or stroke (Williams et al., 2002). These findings suggest that alterations in chemical composition of CeO_2 may have the potential to increase the susceptibility of plaques to rupture without necessarily increasing overall plaque size. At present, given the low biological activity of the parent material and the direction of the association between plaque macrophages and Ce:Zr ratio, it is not possible to state with any confidence that this is due to differences in redox activity. Nevertheless, this observation merits further investigation with other types of redox-modified nanomaterials in experiments with larger groups of $\text{ApoE}^{-/-}$ mice or extended periods of exposure.

Future directions

The use of a systematic series of NPs of a single compound is desirable; however, further studies with more inherently toxic nanomaterials are required to fully address the role of redox activity. Because of the minimal pulmonary and cardiovascular effects observed with the parent material (CeO_2 NPs without Zr-doping), alteration of the redox activity of these CeO_2 NPs may have a limited capacity to subsequently alter toxicity. Metals and metal oxides that have a conduction band energy (E_c) level that overlaps with the cellular redox potential (-4.12 to -4.84 eV) were shown to have the ability to induce oxygen radicals, oxidative stress, and inflammation *in vitro* and *in vivo* (Zhang et al., 2012). Ongoing work in our laboratories will investigate this hypothesis, using a newly synthesized series of metal doped nanoparticles with a conduction band energy that overlaps the cellular redox potential.

Conclusions

This study investigated the pulmonary and cardiovascular effects of redox modification of metal oxide nanoparticles using varying levels of metal doping of a structurally reproducible material. CeO_2 NPs had minimal pulmonary and cardiovascular effects following subacute inhalation at four weeks post-exposure. Zr-doping of CeO_2 NPs had limited effects on these responses, although indications that Zr-doping could potentially alter particle loading of alveolar macrophages and increase the inflammatory cell content in atherosclerosis plaques merit further investigation. Future studies with other types of redox-modified nanomaterials of greater inherent toxicity and a wider range of redox activities are required to fully assess the influence of redox-modification on the toxicity of nanomaterials.

Acknowledgements

The authors would like to thank Paul H.B. Fokkens, Daan L.A.C. Leseman, Liset J.J. de la Fonteyne, Piet K. Beekhof, Christine M.R. Soputan, Hans J.C. Strootman, Jolanda Rijters, Ron F. Vlug, Karin M.P. van den Hurk, Julia Kolling, Geert B. van der Horst, Rory Verhagen, Dirk J. Elberts, Pieter W. Dissel and Angéla Gomersbach-de Ridder for their help during the conduction of the animal experiment and valuable technical assistance. In addition, Geert B. van de Horst is acknowledged for his contribution to the generation of the cytotoxicity in A549 cells and Joost Lensen of Will Research for the histopathology.

Disclosure statement

No potential conflict of interest was reported by the authors.

Funding

The work leading to these results has received funding from the European Union Seventh Framework Programme for research, technology development and demonstration under grant agreement n° 310451 (NanoMILE) and the Netherlands Food and Consumer Product Safety Authority (NVWA).

ORCID

- Mark R. Miller  <http://orcid.org/0000-0002-7078-597X>
 Roel P. F. Schins  <http://orcid.org/0000-0001-5881-6289>
 Isabella Römer  <http://orcid.org/0000-0003-3556-970X>
 Rob J. Vandebril  <http://orcid.org/0000-0001-9140-952X>
 Iseult Lynch  <http://orcid.org/0000-0003-4250-4584>
 Eugenia Valsami-Jones  <http://orcid.org/0000-0002-8850-7556>
 Shea P. Connell  <http://orcid.org/0000-0002-2850-3908>
 Harm J. Heusinkveld  <http://orcid.org/0000-0002-3269-5586>
 Flemming R. Cassee  <http://orcid.org/0000-0001-9958-8630>

References

- Aalapati S, Ganapathy S, Manapuram S, Anumolu G, Prakya BM. 2014. Toxicity and bio-accumulation of inhaled cerium oxide nanoparticles in CD1 mice. *Nanotoxicology* 8:786–98.
- Borm P, Cassee FR, Oberdorster G. 2015. Lung particle overload: old school -new insights? Part *Fibre Toxicol* 12:10.
- Cabanas A, Darr JA, L E, Poliakoff M. 2000. A continuous and clean one-step synthesis of nano-particulate $\text{Ce}_{1-x}\text{Zr}_x\text{O}_2$ solid solutions in near-critical water. *Chem Commun* 2000:901–2.
- Cao Y, Jacobsen NR, Danielsen PH, Lenz AG, Stoeger T, Loft S, et al. 2014. Vascular effects of multiwalled carbon nanotubes in dyslipidemic $\text{ApoE}^{-/-}$ mice and cultured endothelial cells. *Toxicol Sci* 138:104–16.
- Cassee FR, Campbell A, Boere AJ, Mclean SG, Duffin R, Krystek P, et al. 2012. The biological effects of subacute inhalation of diesel exhaust following addition of cerium oxide nanoparticles in atherosclerosis-prone mice. *Environ Res* 115:1–10.
- Cassee FR, Van Balen EC, Singh C, Green D, Muijsen H, Weinstein J, Dreher K. 2011. Exposure, health and ecological effects review of engineered nanoscale cerium and cerium oxide associated with its use as a fuel additive. *Crit Rev Toxicol* 41:213–29.
- Celardo I, De Nicola M, Mandoli C, Pedersen JZ, Traversa E, Ghibelli L. 2011. $\text{Ce}(3+)$ ions determine redox-dependent anti-apoptotic effect of cerium oxide nanoparticles. *ACS Nano* 5:4537–49.
- Chen T, Hu J, Chen C, Pu J, Cui X, Jia G. 2013. Cardiovascular effects of pulmonary exposure to titanium dioxide nanoparticles in ApoE knockout mice. *J Nanosci Nanotechnol* 13:3214–22.
- Coleman R, Hayek T, Keidar S, Aviram M. 2006. A mouse model for human atherosclerosis: long-term histopathological study of lesion development in the aortic arch of apolipoprotein E-deficient (E0) mice. *Acta Histochem* 108:415–24.
- Demokritou P, Gass S, Pyrgiotakis G, Cohen JM, Goldsmith W, McKinney W, et al. 2013. An *in vivo* and *in vitro* toxicological characterisation of realistic nanoscale $\text{CeO}(2)$ inhalation exposures. *Nanotoxicology* 7:1338–50.
- Donovan AR, Adams CD, Ma Y, Stephan C, Eichholz T, Shi H. 2016. Detection of zinc oxide and cerium dioxide nanoparticles during drinking water treatment by rapid single particle ICP-MS methods. *Anal Bioanal Chem* 408:5137–45.
- Dunnick KM, Morris AM, Badding MA, Barger M, Stefaniak AB, Sabolsky EM, Leonard SS. 2016. Evaluation of the effect of valence state on cerium oxide nanoparticle toxicity following intratracheal instillation in rats. *Nanotoxicology* 10:992–1000.
- Dunnick KM, Pillai R, Pisane KL, Stefaniak AB, Sabolsky EM, Leonard SS. 2015. The effect of cerium oxide nanoparticle valence state on reactive oxygen species and toxicity. *Biol Trace Elem Res* 166:96–107.
- Eom HJ, Choi J. 2009. Oxidative stress of CeO_2 nanoparticles via p38-Nrf-2 signalling pathway in human bronchial epithelial cell, Beas-2B. *Toxicol Lett* 187:77–83.

- Fiket Z, Rozmaric M, Krmpotic M, Benedik L. 2015. Levels of major and trace elements, including rare earth elements, and (2)(3)(8)U in Croatian tap waters. *Environ Sci Pollut Res Int* 22:6789–99.
- Fu PP, Xia Q, Hwang HM, Ray PC, Yu H. 2014. Mechanisms of nanotoxicity: generation of reactive oxygen species. *J Food Drug Anal* 22:64–75.
- Geraets L, Oomen AG, Schroeter JD, Coleman VA, Cassee FR. 2012. Tissue distribution of inhaled micro- and nano-sized cerium oxide particles in rats: results from a 28-day exposure study. *Toxicol Sci* 127:463–73.
- Gosens I, Mathijssen LE, Bokkers BG, Muijser H, Cassee FR. 2014. Comparative hazard identification of nano- and micro-sized cerium oxide particles based on 28-day inhalation studies in rats. *Nanotoxicology* 8:643–53.
- Grainger DJ, Reckless J, Mckilligan E. 2004. Apolipoprotein E modulates clearance of apoptotic bodies in vitro and in vivo, resulting in a systemic proinflammatory state in apolipoprotein E-deficient mice. *J Immunol* 173:6366–75.
- Greim H, Ziegler-Sklakakis K. 2007. Risk assessment for biopersistent granular particles. *Inhal Toxicol* 19 Suppl 1:199–204.
- He W, Liu Y, Wamer WG, Yin JJ. 2014. Electron spin resonance spectroscopy for the study of nanomaterial-mediated generation of reactive oxygen species. *J Food Drug Anal* 22:49–63.
- Hirst SM, Karakoti AS, Tyler RD, Sriranganathan N, Seal S, Reilly CM. 2009. Anti-inflammatory properties of cerium oxide nanoparticles. *Small* 5:2848–56.
- Kang GS, Gillespie PA, Gunnison A, Moreira AL, Tchou-Wong KM, Chen LC. 2011. Long-term inhalation exposure to nickel nanoparticles exacerbated atherosclerosis in a susceptible mouse model. *Environ Health Perspect* 119:176–81.
- Keller J, Wohlleben W, Ma-Hock L, Strauss V, Grotters S, Kuttler K, et al. 2014. Time course of lung retention and toxicity of inhaled particles: short-term exposure to nano-Ceria. *Arch Toxicol* 88:2033–59.
- Kunzli N, Perez L, Von Klot S, Baldassarre D, Bauer M, Basagana X, et al. 2011. Investigating air pollution and atherosclerosis in humans: concepts and outlook. *Prog Cardiovasc Dis* 53:334–43.
- Landsiedel R, Sauer UG, Ma-Hock L, Schnekenburger J, Wiemann M. 2014. Pulmonary toxicity of nanomaterials: a critical comparison of published in vitro assays and in vivo inhalation or instillation studies. *Nanomedicine (Lond)* 9:2557–85.
- Leung YH, Yung MM, Ng AM, Ma AP, Wong SW, Chan CM, et al. 2015. Toxicity of CeO₂ nanoparticles - the effect of nanoparticle properties. *J Photochem Photobiol B* 145:48–59.
- Li Z, Hulderman T, Salmen R, Chapman R, Leonard SS, Young SH, et al. 2007. Cardiovascular effects of pulmonary exposure to single-wall carbon nanotubes. *Environ Health Perspect* 115:377–82.
- Lin W, Huang YW, Zhou XD, Ma Y. 2006. Toxicity of cerium oxide nanoparticles in human lung cancer cells. *Int J Toxicol* 25:451–7.
- Mikkelsen L, Sheykhzade M, Jensen KA, Saber AT, Jacobsen NR, Vogel U, et al. 2011. Modest effect on plaque progression and vasodilatory function in atherosclerosis-prone mice exposed to nanosized TiO₂. *Part Fibre Toxicol* 8:32.
- Miller MR, Mclean SG, Duffin R, Lawal AO, Araujo JA, Shaw CA, et al. 2013. Diesel exhaust particulate increases the size and complexity of lesions in atherosclerotic mice. *Part Fibre Toxicol* 10:61.
- Miller MR, Shaw CA, Langrish JP. 2012. From particles to patients: oxidative stress and the cardiovascular effects of air pollution. *Future Cardiol* 8:577–602.
- Moller P, Mikkelsen L, Vesterdal LK, Folkmann JK, Forchhammer L, Roursgaard M, et al. 2011. Hazard identification of particulate matter on vasomotor dysfunction and progression of atherosclerosis. *Crit Rev Toxicol* 41:339–68.
- Morimoto Y, Izumi H, Yoshiura Y, Tomonaga T, Oyabu T, Myojo T, et al. 2015. Pulmonary toxicity of well-dispersed cerium oxide nanoparticles following intratracheal instillation and inhalation. *J Nanopart Res* 17:442.
- Naura AS, Hans CP, Zerfaoui M, Errami Y, Ju J, Kim H, et al. 2009. High-fat diet induces lung remodeling in ApoE-deficient mice: an association with an increase in circulatory and lung inflammatory factors. *Lab Invest* 89:1243–51.
- Niwa Y, Hiura Y, Murayama T, Yokode M, Iwai N. 2007. Nano-sized carbon black exposure exacerbates atherosclerosis in LDL-receptor knockout mice. *Circ J* 71:1157–61.
- Park EJ, Choi J, Park YK, Park K. 2008. Oxidative stress induced by cerium oxide nanoparticles in cultured BEAS-2B cells. *Toxicology* 245:90–100.
- Pesic M, Podolski-Renic A, Stojkovic S, Matovic B, Zmejkoski D, Kojic V, et al. 2015. Anti-cancer effects of cerium oxide nanoparticles and its intracellular redox activity. *Chem Biol Interact* 232:85–93.
- Pisoschi AM, Pop A. 2015. The role of antioxidants in the chemistry of oxidative stress: a review. *Eur J Med Chem* 97:55–74.
- Slob W. 2002. Dose-response modeling of continuous endpoints. *Toxicol Sci* 66:298–312.
- Srinivas A, Rao PJ, Selvam G, Murthy PB, Reddy PN. 2011. Acute inhalation toxicity of cerium oxide nanoparticles in rats. *Toxicol Lett* 205:105–15.
- Tsai YY, Oca-Cossio J, Lin SM, Woan K, Yu PC, Sigmund W. 2008. Reactive oxygen species scavenging properties of ZrO₂–CeO₂ solid solution nanoparticles. *Nanomedicine (Lond)* 3:637–45.
- Unfried K, A C, Klotz L-O, Von Mikecz A, Susanne G-B, Schins RPF. 2007. Cellular responses to nanoparticles: target structures and mechanisms. *Nanotoxicology* 1:52–71.
- Williams H, Johnson JL, Carson KG, Jackson CL. 2002. Characteristics of intact and ruptured atherosclerotic plaques in brachiocephalic arteries of apolipoprotein E knockout mice. *Arterioscler Thromb Vasc Biol* 22:788–92.
- Xia T, Kovochich M, Liang M, Madler L, Gilbert B, Shi H, et al. 2008. Comparison of the mechanism of toxicity of zinc oxide and cerium oxide nanoparticles based on dissolution and oxidative stress properties. *ACS Nano* 2:2121–34.
- Xue Y, Zhai Y, Zhou K, Wang L, Tan H, Luan Q, Yao X. 2012. The vital role of buffer anions in the antioxidant activity of CeO₂ nanoparticles. *Chemistry* 18:11115–22.
- Yokel RA, Au TC, Macphail R, Hardas SS, Butterfield DA, Sultana R, et al. 2012. Distribution, elimination, and biopersistence to 90 days of a systemically introduced 30 nm ceria-engineered nanomaterial in rats. *Toxicol Sci* 127:256–68.
- Yokel RA, Tseng MT, Dan M, Unrine JM, Graham UM, Wu P, Grulke EA. 2013. Biodistribution and biopersistence of ceria engineered nanomaterials: size dependence. *Nanomedicine* 9:398–407.
- Zhang H, Ji Z, Xia T, Meng H, Low-Kam C, Liu R, et al. 2012. Use of metal oxide nanoparticle band gap to develop a predictive paradigm for oxidative stress and acute pulmonary inflammation. *ACS Nano* 6:4349–68.